# On the influence of glass fiber mat on the mixed-mode fracture of composite-to-metal bonded joints

Moreira Arouche, Marcio; Teixeira de Freitas, Sofia; de Barros, Silvio

**DOI**
10.1016/j.compstruct.2020.113109

**Publication date**
2021

**Document Version**
Final published version

**Published in**
Composite Structures

**Citation (APA)**
Moreira Arouche, M., Teixeira de Freitas, S., & de Barros, S. (2021). On the influence of glass fiber mat on the mixed-mode fracture of composite-to-metal bonded joints. *Composite Structures*, *256*, Article 113109. https://doi.org/10.1016/j.compstruct.2020.113109

Composite Structures 256 (2021) 113109

Contents lists available at ScienceDirect

Composite Structures

journal homepage: www.elsevier.com/locate/compstruct

# On the influence of glass fiber mat on the mixed-mode fracture of composite-to-metal bonded joints

Marcio Moreira Arouche [a,b], Sofia Teixeira de Freitas [b,*], Silvio de Barros [a,c]

[a] Federal Center for Technological Education of Rio de Janeiro - CEFET/RJ, Av. Maracanã 229, 20271-110, Rio de Janeiro, Brazil
[b] Delft University of Technology, Kluyverweg 1, 2629HS, Delft, Netherlands
[c] GeM Institute, UMR 6183 CNRS, CESI, Saint-Nazaire, France

ARTICLE INFO

*Keywords:*
Mixed-mode bending (MMB)
Bi-material bonded joints
Toughening mechanism
Surface roughness
Fractography

ABSTRACT

In this work, the influence of a layer of glass fiber mat (GFM) inserted in a bi-material bonded joint interface is investigated as a toughening mechanism to improve the fracture performance of bonded structures. Composite-to-metal bonded specimens were manufactured by hand lay-up using two different consolidation processes: at room pressure or using vacuum bagging. The fracture behavior was evaluated under quasi-static loadings using the mixed-mode bending (MMB) test. Test results revealed an increase of the fracture toughness with the insertion of an adjacent layer of GFM. The toughening mechanism is associated with a more irregular fracture surface profile. It was verified a relationship between the fracture surface roughness and the fracture toughness. The toughening effect showed to be more evident in higher mode II fracture conditions. The insertion of a layer of GFM and the use of vacuum pressure in the consolidation of the composite increase the fracture performance of composite repairs in metal structures.

## 1. Introduction

The requirement of lightweight structures has encouraged the introduction of composite materials in industrial applications [1]. First applications of composite structures are found in aerospace industry [2,3] and have been expanded to many other fields, such as automotive [4] and construction [5]. Adhesive bonding technology is generally the preferred joining method for composite structures as they provide enhanced stress transfer mechanisms and design flexibility [6]. The selection of the manufacturing method usually depends on the analysis of several parameters, such as substrates to be bonded, service conditions and area of application [1,7–9].

Recently, composite materials technology has been introduced to the maintenance routine in offshore industry [10]. Oil and gas production platforms are projected to remain more than 20 years in operation. The floating vessels are subjected to harsh environment and a large maintenance routine is necessary in order to ensure structural integrity and continuous production. During the life cycle of a plant, repairs on metallic structures are crucial as result of corrosion and fatigue degradation. The composite repair technology arises as a promising alternative for the rehabilitation of pipes [10,11], tanks [12] and ship hull [13]. The technology has the advantage of avoiding hot work, which is safer and does not require to stop the production. A composite patch is bonded to a damaged metallic structure in order to re-establish the structural integrity. In the repair, a carbon fiber composite patch is usually manufactured using hand lay-up [14]. This leads to new applications of adhesively bonded structures between composite and metal adherends.

The fracture mechanics approach is widely applied to improve the design and evaluate the performance of structures. In the cases of delamination and debonding, cracks usually propagate along an interface. In real-life applications, interfacial fracture often propagates in a combination of opening (mode I) and shear (mode II) loadings. A variety of experimental procedures is available for mixed-mode fracture testing [15]. Among them, the mixed-mode bending (MMB) test [16,17] stands out for its easy implementation and capability of testing a wide range of partitioning ratios with only one specimen geometry. The MMB test method was originally developed for fracture propagation of unidirectional symmetric composites and was later extended to multidirectional laminates [18,19], metal bonded joints [20,21], sandwich specimen face/core debonding [22] and bi-material bonded joints [23].

The crack propagation path in a bonded structure depends on the fracture resistance of the adherends, the interface toughness and the

* Corresponding author.
*E-mail addresses:* marcio.m.arouche@gmail.com (M. Moreira Arouche), s.teixeiradefreitas@tudelft.nl (S. Teixeira de Freitas), silvio.debarros@gmail.com (S. de Barros).

https://doi.org/10.1016/j.compstruct.2020.113109
Received 6 March 2020; Revised 24 June 2020; Accepted 4 October 2020
Available online 13 October 2020

applied fracture mode ratio [24]. An interfacial crack in a composite bonded structure may kink into the composite adherend. Crack migration is encouraged by a relatively low delamination fracture toughness of the composite material compared to the interface and high shear loadings at the crack tip. In these cases, the bonded interface does not influence the fracture toughness. Instead, an interlaminar fracture occurs and the adjacent composite layer to the bonded interface has an important role in the fracture performance of the structure [25]. The fracture performance of a composite laminate may be increased by design optimization of the lay-up sequence [26]. However, the development of composite toughening methods has a greater potential for surpassing the limitations of the current material systems [27]. The choice of a toughening method depends on the structural requirements, in-service conditions and available manufacturing technology.

Kuwata and Hogg investigated the toughening effect of interleaved fiber veils on a carbon fiber reinforced polymer (CFRP) under pure mode I fracture [28]. They associated the toughening mechanism to the effect of fiber-bridging. The work of Hosseini et al. [29] revealed a decrease in the pure mode I fracture toughness of a woven glass/epoxy composite with an inserted glass fiber chopped strand mat at the delamination interface. Regarding the pure mode II fracture, toughening mechanisms are less dependent on fiber bridging and more affected by additional factors beyond the material of the delamination interface [30]. However, these studies address only the pure modes and a limited combination of bonded materials. Additional studies are required in order to understand the fracture toughening mechanisms and improve the performance of structures.

Boccaccini and Winkler [31] correlated the increase in the fracture toughness of a composite with a crack deflection mechanism. An experimental study in sandwich structures showed that the fracture toughness can be increased by inserting a layer of mat with randomly oriented fibers between the adherends [32]. Karger-Kocsis et al. [33] obtained higher fracture stresses and enlarged damage zone in a polypropylene composite with glass fiber mat compared with long glass fiber reinforcement. Huang et al. [34] analyzed the interlaminar toughening of carbon-fiber/epoxy composite laminates with chopped aramid fibers. Kopp et al. [35] showed that the topography of the fracture surfaces has an intrinsic effect in the fracture characterization of materials. Sun et al. [36] obtained higher fracture toughness in a composite-to-metal bonded joint by interleaving short aramid fibers and altering surface treatments. These works suggest that the fracture surfaces profile of the delamination interface has an important role in the performance of the structure.

Present literature does not fully address the toughening mechanisms associated to the use of a mat in bonded joints, particularly under mixed-mode fracture conditions. A detailed analysis is required in order to describe the toughening effect in new applications of bonded structures. In this work, the influence of a layer of glass fiber mat (GFM) in the fracture performance of a bi-material bonded joint is investigated. Composite-to-metal bonded specimens are manufactured by hand lay-up with two different consolidation processes: at room pressure or using vacuum bagging. The mixed-mode fracture behavior is assessed under quasi-static loadings using the MMB test. The crack propagation mechanisms resulted from the insertion of a layer of GFM between the adherends are verified with a fracture surface analysis.

## 2. Materials and methods

### 2.1. Specimen design and manufacture

Composite-to-metal bonded specimens were manufactured in order to simulate the application of a composite repair to a metal structure in offshore industry [14]. A carbon steel plate (ASTM A36) of 3.18 mm thickness was selected for the metal adherend. The steel surface was blasted with steel grit (G-40) and degreased with acetone. An anti-friction material was applied in order to produce a pre-cracked region. Then, an epoxy adhesive (NVT201E, Novatec, Rio de Janeiro, Brazil) with a glass transition temperature (Tg) of 80 °C was applied. One layer of glass fiber chopped strand mat with a density of 300 g/m$^2$ was inserted between the adherends on half of the plate. Bidirectional carbon fiber fabrics (LTC450-C10-C, DEVOLD AMT, LangevÔg, Norway) with density of 430 g/m$^2$ and epoxy lamination resin (PIPEFIX, Polinova S.A., Rio de Janeiro, Brazil) with a Tg of 116 °C and working life of 30 min. were selected for the composite adherend.

Two CFRP-to-steel plates were manufactured by hand lay-up of carbon fiber fabrics on the treated steel surface. Hand rollers are used to compact the composite layers. The first plate is consolidated at room pressure and has a total of 10 layers of 0/90 carbon fibers. The second plate was consolidated using vacuum bagging. In this case, 12 layers of 0/90 carbon fibers were laminated in order to produce a similar composite thickness after curing. The layer of 0° carbon fibers adjacent to the adhesive interface was placed at the length direction and the cure process took approximately 2 h at room temperature. Mechanical properties of the are presented in Table 1.

Specimens were cut from the plates and measured with a digital caliper from three different regions: 30 mm from the sides and at center of the specimens. The length was obtained with a ruler. Table 2 shows the average measurements of the different specimen configurations: manufactured at room pressure without glass fiber mat (RP) and with glass fiber mat (RP/GFM); and manufactured using vacuum bagging without (VB) and with glass fiber mat (VB/GFM).

### 2.2. Experimental method

The mixed-mode bending (MMB) test was chosen for the experimental mixed-mode fracture analysis of the specimens. In the MMB test, a loading is applied through a roller attached to a lever and loaded just above the mid-plane of the test specimen. The test loading (P) is decomposed in opening ($P_I$) and shear ($P_{II}$) loadings in a constant ratio determined by the lever length (c), as shown in Fig. 1. The mode I fracture ratio increases with the lever length. The lever weight produces a load ($P_g$) on the specimen at the length of the lever center of gravity ($c_g$). The test half-span (L) is set to 70 mm and the initial crack length (a) is 30 mm.

Tests were conducted using a servo-hydraulic testing machine (MTS 831, MTS Systems Corporation, United States of America) coupled with a 10 kN load cell. The testing loads were applied with displacement control at the quasi-static rate of 0.5 mm/min. Table 3 shows the test configurations. Specimens were tested in 75% and 40% mode II fracture ratio. The fracture partitioning ratio was obtained from a finite element model created in a previous work [23]. Load-displacement points were obtained during the test and a high-resolution camera was positioned for crack length monitoring.

## 3. Results

Load-displacement curves were obtained from the tests. Tests were performed until the crack length reached 65 mm and the propagation points were obtained in each 1 mm crack step. Some non-linearity may be noticed in the beginning of the test due to the initial load distribution on the testing apparatus. Results of specimens manufactured at room pressure and tested under 75% mode II fracture are shown in Fig. 2. A stepwise crack propagation is observed in the specimens with an inserted layer of GFM. Regarding the specimens without GFM, a more abrupt load drop occurred in three of the tests while only test RP-2 presented a stepwise propagation. Specimens with GFM presented slightly higher testing loadings compared with the specimens without GFM.

Fig. 3 shows the results of specimens manufactured using vacuum bagging and tested under 75% mode II fracture. All tests presented

**Table 1**
Mechanical properties of the materials [37].

| Material | E; $E_1$ (GPa) | $E_2$ (GPa) | $G_{12}$ (GPa) | ν; $\nu_{12}$ |
|---|---|---|---|---|
| Carbon steel | 200 | – | – | 0.27 |
| Adhesive | 2.25 | – | – | 0.38 |
| Carbon-epoxy ply | 82 | 10 | 3.0 | 0.24 |

**Table 2**
Specimen measurements.

| Specimens | Manufacture Process | Design | Thickness (mm) | Width (mm) | Length (mm) |
|---|---|---|---|---|---|
| RP | room pressure | without GFM | 9.49 ± 0.34 | 25.11 ± 0.11 | 180 ± 1 |
| RP/GFM | room pressure | with GFM | 9.82 ± 0.45 | 25.31 ± 0.14 | 180 ± 1 |
| VB | vacuum bagging | without GFM | 9.95 ± 0.27 | 25.08 ± 0.14 | 180 ± 1 |
| VB/GFM | vacuum bagging | with GFM | 10.07 ± 0.36 | 25.29 ± 0.10 | 180 ± 1 |

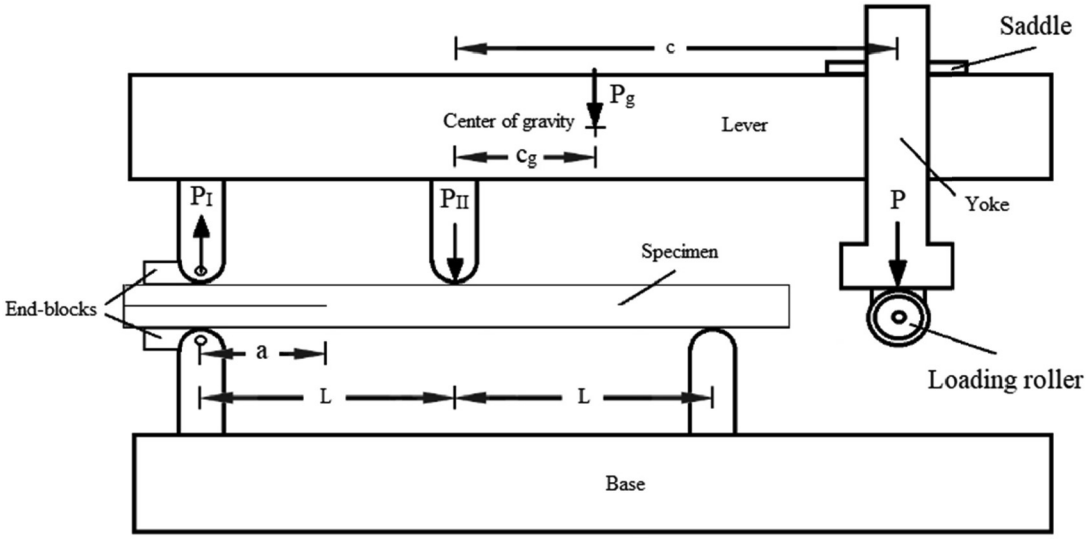


**Fig. 1.** MMB test scheme.

**Table 3**
Test matrix.

| Test | Specimen | Manufacture Process | Design | Lever length, c (mm) | $G_{II}/G$ |
|---|---|---|---|---|---|
| 1 | RP-1 | room pressure | without GFM | 42 | 75% |
| 2 | RP-2 | room pressure | without GFM | 42 | 75% |
| 3 | RP-3 | room pressure | without GFM | 42 | 75% |
| 4 | RP-4 | room pressure | without GFM | 42 | 75% |
| 5 | RP/GFM-1 | room pressure | with GFM | 42 | 75% |
| 6 | RP/GFM-2 | room pressure | with GFM | 42 | 75% |
| 7 | RP/GFM-3 | room pressure | with GFM | 42 | 75% |
| 8 | RP/GFM-4 | room pressure | with GFM | 42 | 75% |
| 9 | VB-1 | vacuum bagging | without GFM | 42 | 75% |
| 10 | VB-2 | vacuum bagging | without GFM | 42 | 75% |
| 11 | VB-3 | vacuum bagging | without GFM | 42 | 75% |
| 12 | VB/GFM-1 | vacuum bagging | with GFM | 42 | 75% |
| 13 | VB/GFM-2 | vacuum bagging | with GFM | 42 | 75% |
| 14 | VB/GFM-3 | vacuum bagging | with GFM | 42 | 75% |
| 15 | VB-4 | vacuum bagging | without GFM | 110 | 40% |
| 16 | VB-5 | vacuum bagging | without GFM | 110 | 40% |
| 17 | VB/GFM-4 | vacuum bagging | with GFM | 110 | 40% |
| 18 | VB/GFM-5 | vacuum bagging | with GFM | 110 | 40% |

abrupt load drop during crack propagation. Specimens with an inserted layer of GFM had significant higher test loadings compared to specimens without GFM. Tests were also performed under 40% mode II ratio fracture configuration and the results are shown in Fig. 4. In this condition, all tests presented a smooth variation of the test load during crack propagation. Specimens with an inserted layer of GFM presented slightly higher loadings in compared to the specimens without GFM. Overall, the insertion of a layer of GFM between

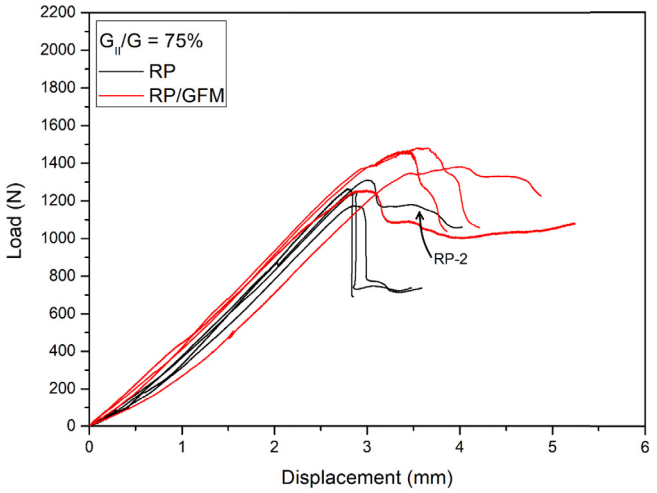


**Fig. 2.** Load-displacement curves of specimens manufactured at room pressure under 75% mode II fracture.

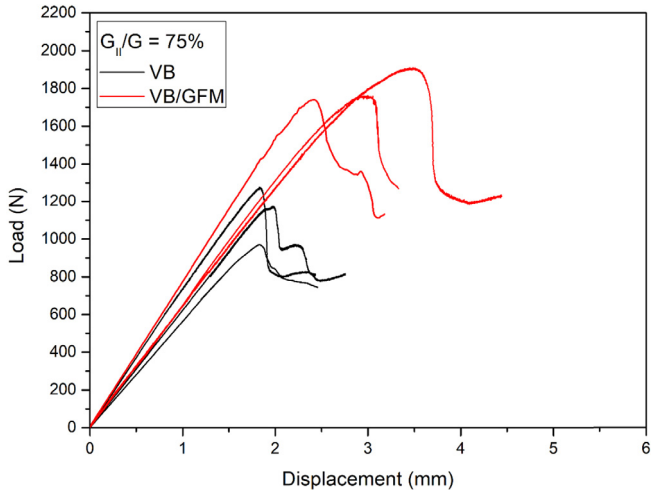


**Fig. 3.** Load-displacement of specimens manufactured using vacuum bagging under 75% mode II fracture.

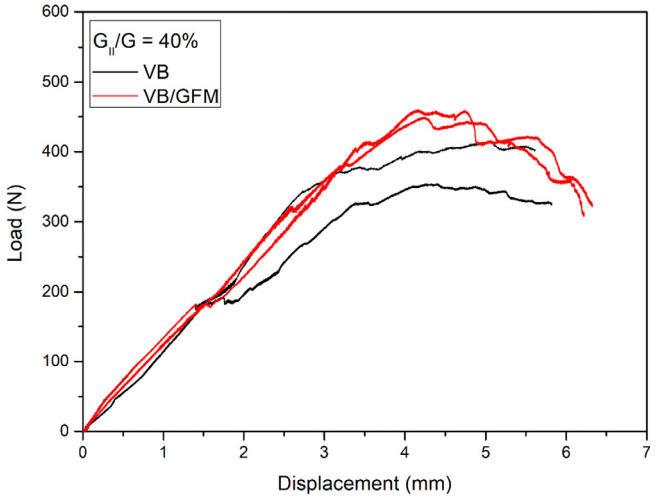


**Fig. 4.** Load-displacement of specimens manufactured using vacuum bagging under 40% mode II fracture.

adherends increased the fracture loadings of the bonded joints although in different degree depending on the manufacture process and fracture mode ratio.

Images of the fracture propagation paths were obtained from an optical microscope. Fig. 5 shows the typical fracture propagation paths of the specimens without GFM and with a layer of GFM between adherends. Crack migration was observed in all tests. This is attributed to the higher stresses in the upper arm of the specimen caused by the MMB loading configuration. Consequently, crack propagated within the interface between the adhesive layer and the first layer of the composite adherend with fibers at length direction, as observed in Fig. 5a. The insertion of a layer of GFM between the adherends produced a preferential layer for crack propagation with more irregular path, as seen in Fig. 5b. This suggests an influence of the fracture surface profile on the higher test loadings produced in specimens with GFM. The test results support previous literature regarding the crucial role of the adjacent layer to the adhesive in the fracture performance of the structure [25,26,32–34].

## 4. Discussion

### 4.1. Fracture toughness

Linear elastic fracture mechanics (LEFM) is valid as long as the energy dissipated on the plastic zone developed around the crack tip is in a small scale in relation to the macroscopic elastic response. In this work, the tested specimens have relatively thick adherends which increase the elastic response on a macroscopic scale. Moreover, the use of a brittle epoxy adhesive contributes for a smaller plastic zone. Therefore, the total fracture energy (G) can be calculated from the crack propagation points using simple beam analysis. This approach has been successfully applied in the characterization of composite [19], metal [21] and bi-material [23] bonded joints. The total fracture energy is obtained from the following equation:

$$G = \frac{1}{2B}\left(\frac{M_1^2}{E_1 I_1} + \frac{M_2^2}{E_2 I_2} - \frac{(M_1 + M_2)^2}{EI}\right) \quad (1)$$

where $M_1$ and $M_2$ are the bending moments on the section of the crack tip in the upper and lower arms, respectively, and B is the specimen width. $E_1$, $I_1$, $E_2$, $I_2$, E and I are the flexural moduli and second moments

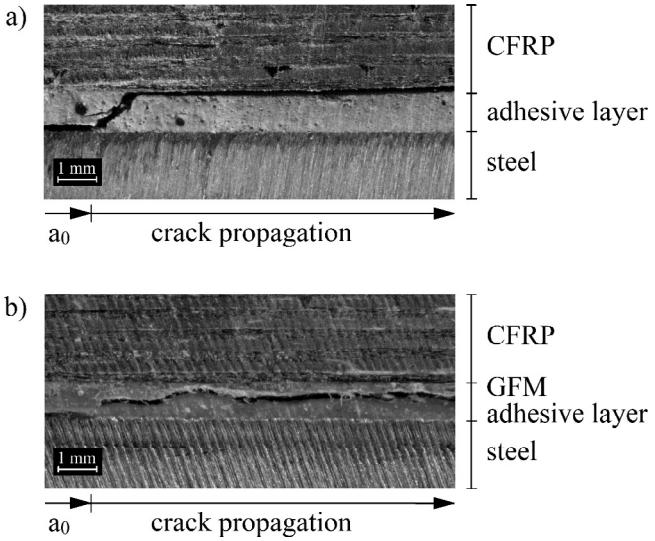


**Fig. 5.** Crack propagation paths of (a) specimens without GFM and (b) specimens with GFM.

of the area in the section of the crack tip of the upper arm, lower arm and total specimen, respectively.

Fig. 6 shows the R-curves of the specimens manufactured at room pressure under 75% mode II fracture. Results were obtained from crack lengths between 35 and 65 mm. The fracture energy increased substantially with the crack length in specimens with GFM although the fracture mode ratio remains constant during the test. This can be explained by the crack deflection mechanism [31] resulted from the more irregular crack path. Specimens with an inserted layer of GFM presented higher fracture energy during propagation when compared with the specimens without GFM. This reveals the toughening effect caused by the insertion of a layer of GFM between the adherends. A note is given to specimen RP-2 which presented similar results to the specimens with GFM. This will be discussed later in this work.

Fig. 7 shows the R-curves obtained from specimens manufactured using vacuum bagging and tested under 75% mode II fracture. Specimens with an inserted layer of GFM presented substantially higher fracture energy compared with the specimens without GFM. The toughening effect is shown to be more significant in specimens manufactured using vacuum bagging. The R-curves from tests under 40% mode II fracture are shown in Fig. 8. In this configuration, both specimens without and with GFM presented similar fracture energy.

These experimental results show that the increase in mode I fracture ratio reduced the toughening effect of the GFM. This shows that the toughening mechanism is not only influenced by the specimen design but also the loading conditions. The relationship between the fracture mode ratio and the toughening effect agrees with literature regarding mat-interlayered composites under pure mode I [29] and pure mode II [30] fracture. A more irregular crack propagation path improves the toughening effect as the shear becomes the dominant fracture mode.

A comparison between the average fracture energy ($G_{ave}$) of the tested specimens is given in Fig. 9. The insertion of a layer of GFM between adherends is shown to increase the fracture energy in both manufacturing processes under 75% mode II fracture. However, the toughening effect is more substantial in specimens manufactured using vacuum bagging when compared to room pressure. Regarding the fracture mode, the GFM produced greater improvement in the vacuum bagging configuration under high mode II condition. Both the manufacturing process and the fracture mode ratio showed to have significant influence in the toughening effect. Moreover, specimens without GFM presented similar fracture energy although it is slightly higher in specimens manufactured using vacuum bagging tested under high mode I fracture.

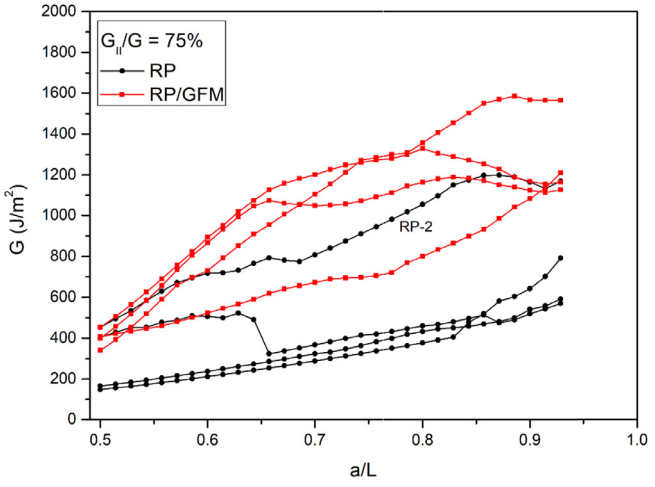


**Fig. 6.** Fracture toughness of specimens manufactured at room pressure under 75% mode II fracture.

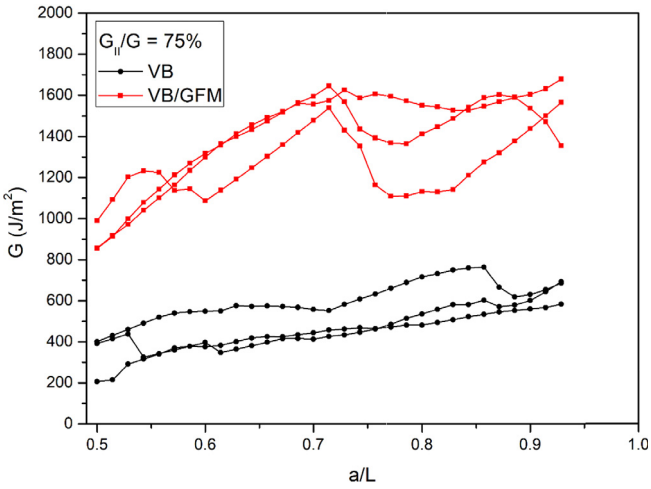


**Fig. 7.** Fracture toughness of specimens manufactured using vacuum bagging under 75% mode II fracture.

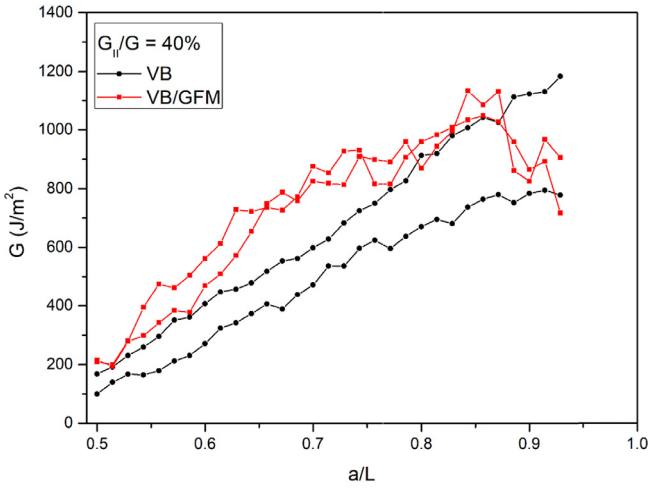


**Fig. 8.** Fracture toughness of specimens manufactured using vacuum bagging under 40% mode II fracture.

### 4.2. Surface profile

An analysis of the fracture surface features was performed using a 3D wide-area measuring optical microscope (Keyence VR-3200, Japan). Fracture surfaces and height profiles were analyzed. The height profiles of the fracture surfaces were obtained from three different paths: center of the surfaces and near the edges on the left and right sides. The aim is to evaluate the influence of the fracture surface profile on the toughening mechanism.

Fig. 10 shows representative images of the fracture surfaces of specimens manufactured at room pressure under 75% mode II fracture. The specimen without GFM (RP-4) presented a crack propagation between the adhesive layer and the adjacent layer of carbon fibers. Otherwise, the specimen with GFM (RP/GFM-2) showed a combination of fracture propagation within the GFM and interlaminar fracture within the adjacent layer of carbon fibers. Representative height profiles are shown in Fig. 11. It reveals a more irregular fracture surface in the specimen with GFM. Crack propagation along irregular paths are shown to require more energy to propagate [31]. This explains the higher fracture toughness of the specimens with GFM.

Fig. 12 shows representative images of the fracture surfaces of specimens manufactured using vacuum bagging under 75% mode II frac-

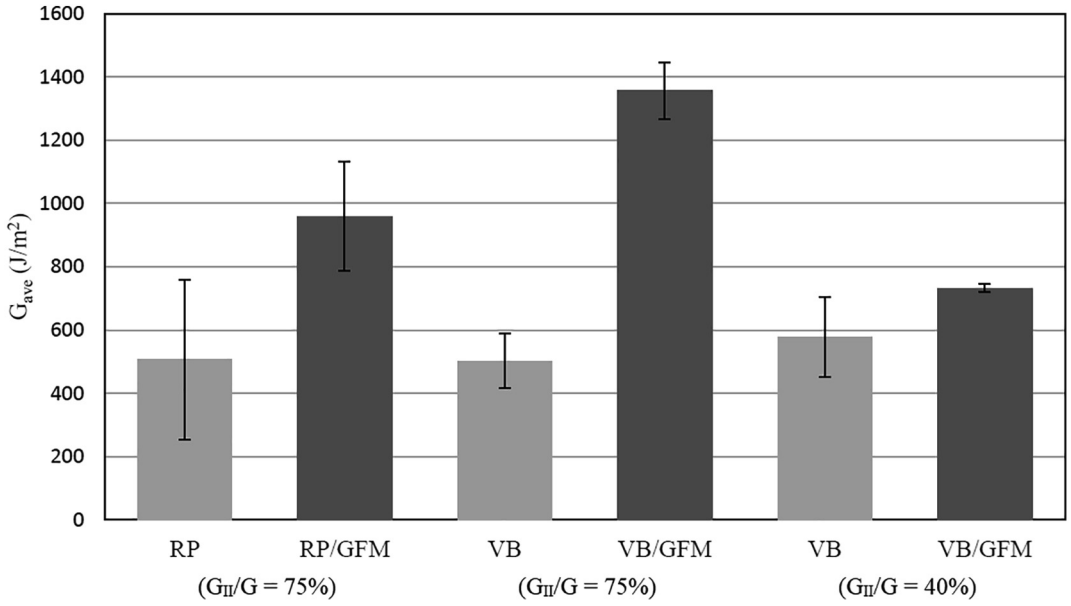


**Fig. 9.** Average fracture energy.

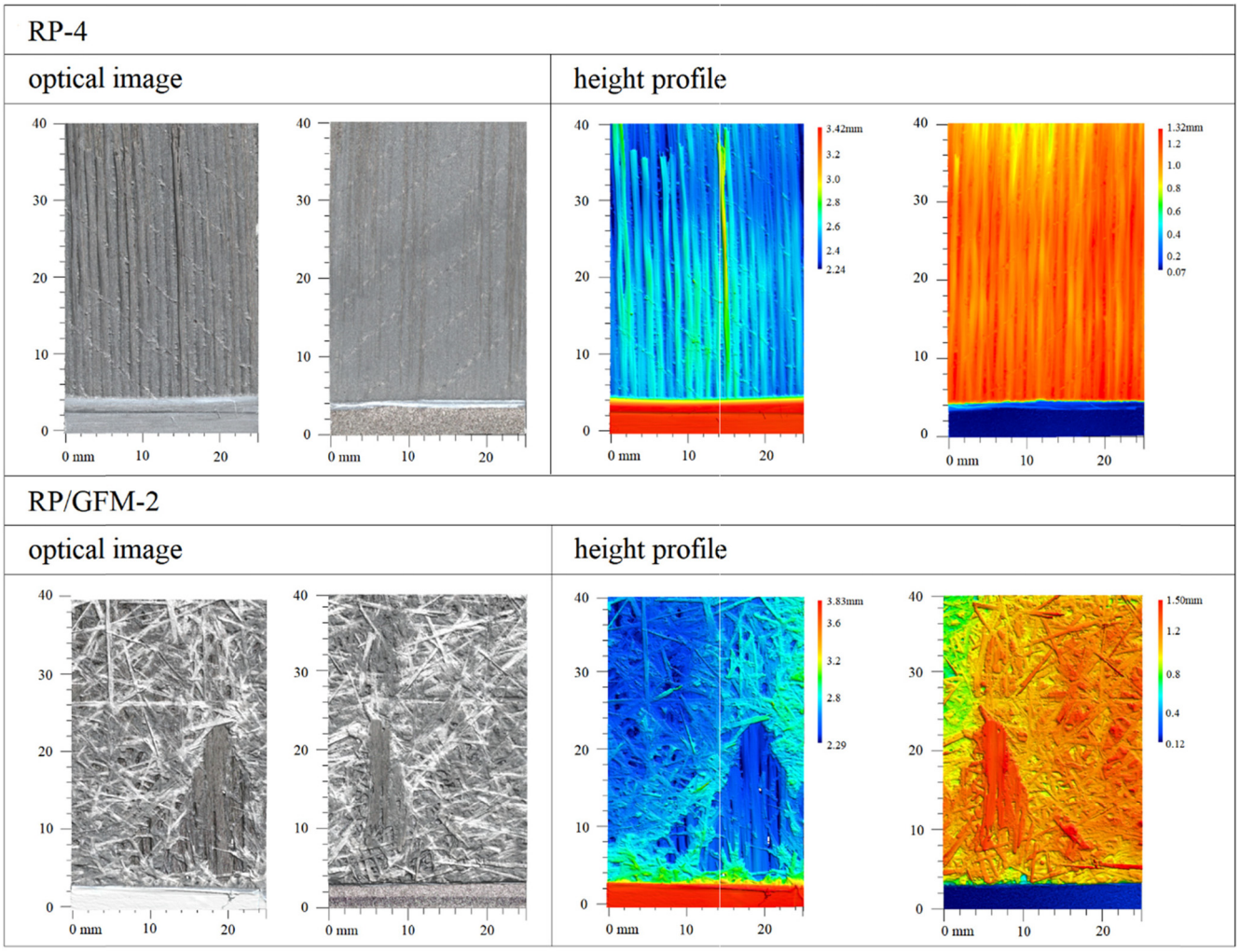


**Fig. 10.** Representative fracture surfaces of specimens manufactured at room pressure under 75% mode II fracture.

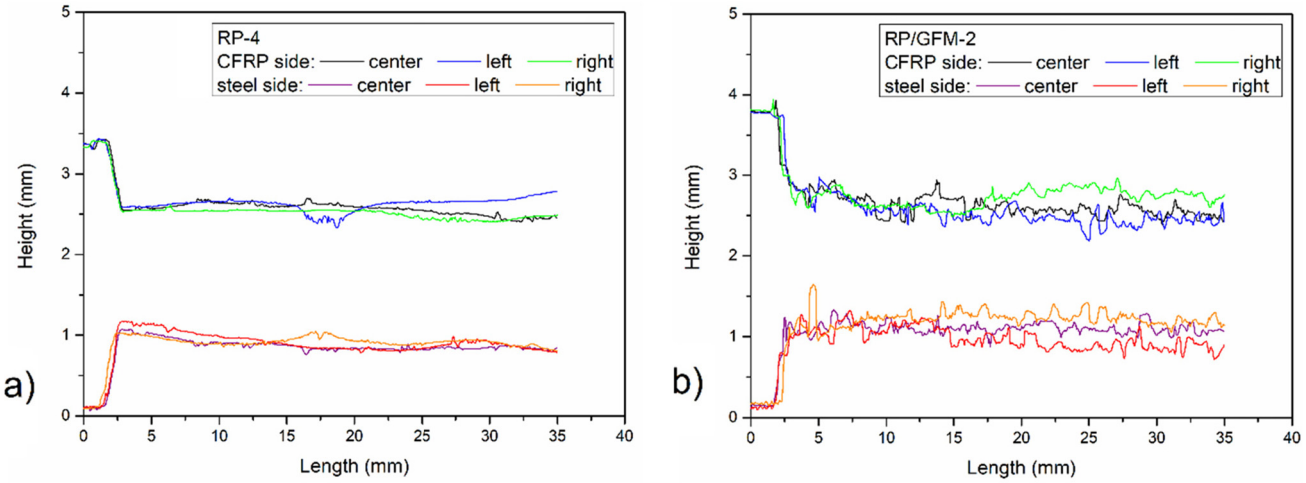


**Fig. 11.** Representative fracture height profiles of specimens manufactured at room pressure under 75% mode II fracture (a) without and (b) with GFM.

ture. The specimen without GFM (VB-2) presented a fracture between the adhesive layer and the adjacent layer of carbon fibers, similar to the specimen manufactured at room pressure (see Fig. 10). However, the specimen with GFM (VB/GFM-3) revealed mostly fracture propagation within the layer of GFM. Representative height profiles are shown in Fig. 13. It reveals a more irregular fracture surface in the specimen with GFM. These results are similar to the specimens manufactured at room pressure (see Fig. 11). Therefore, the manufacturing

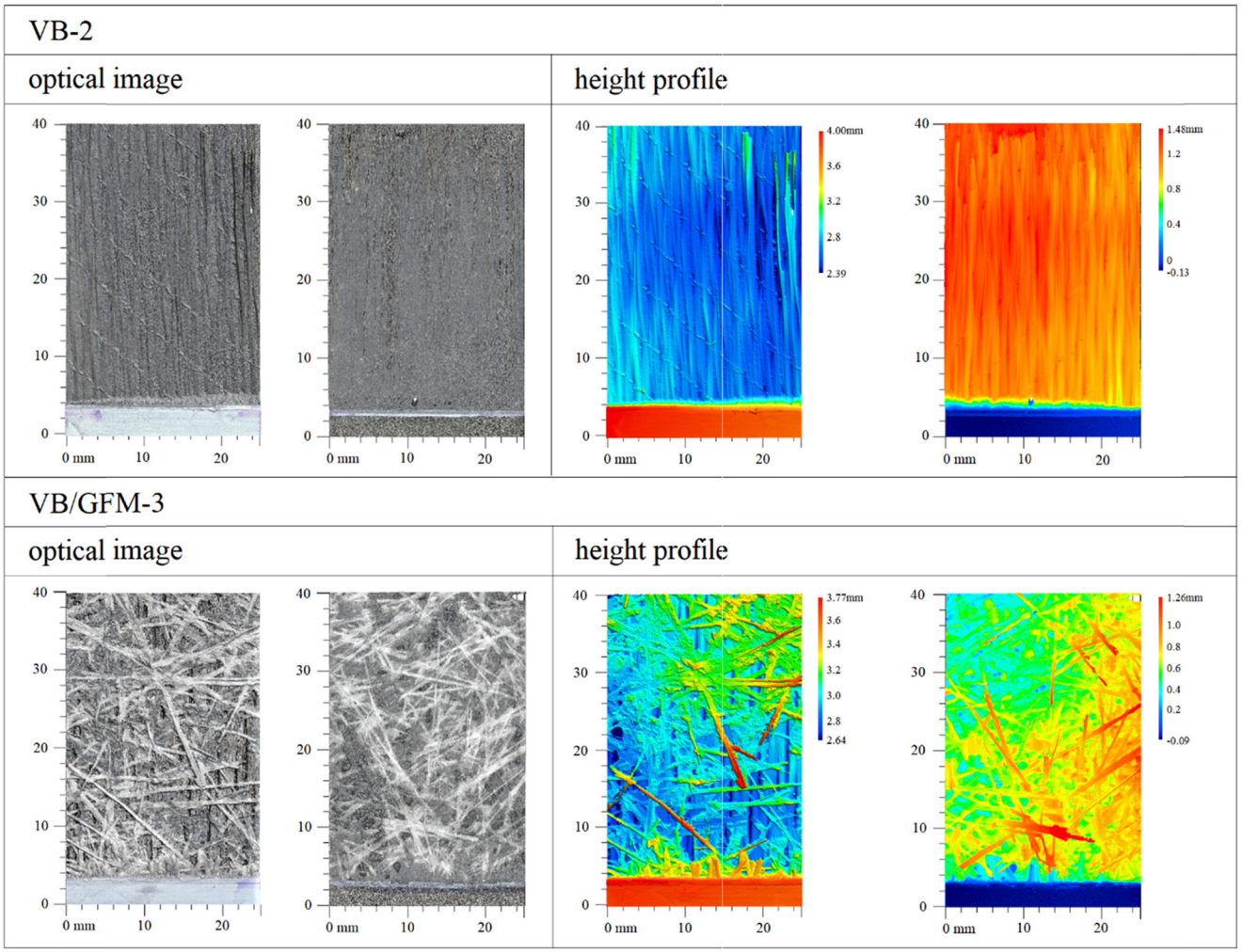


**Fig. 12.** Representative fracture surfaces of specimens manufactured using vacuum bagging under 75% mode II fracture.

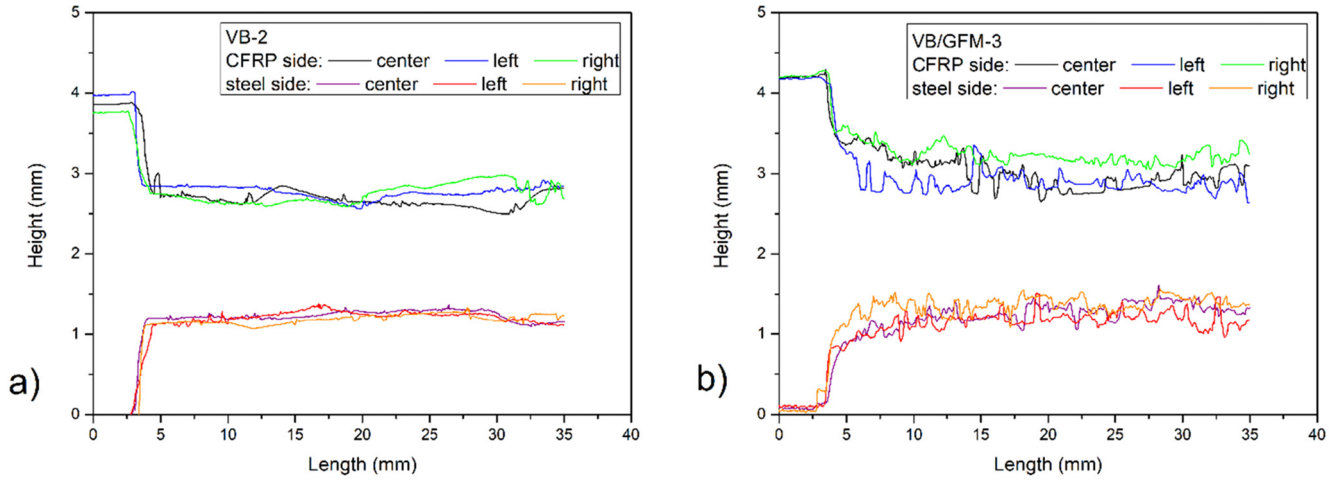


**Fig. 13.** Representative fracture height profiles of specimens manufactured using vacuum bagging under 75% mode II fracture (a) without and (b) with GFM.

process had no notable effect in the height profile of the fracture surfaces.

Fig. 14 shows representative images of the fracture surfaces of specimens manufactured using vacuum bagging under 40% mode II fracture. The specimen without GFM (VB-5) presented a fracture similar to the previous cases of 75% mode II at room pressure (see Fig. 10) or using vacuum bagging (see Fig. 12). Likewise, the specimen with GFM (VB/GFM-5) revealed a fracture propagation within the layer of GFM. Representative height profiles are shown in Fig. 15. They reveal a more irregular fracture surface in the specimen with GFM.

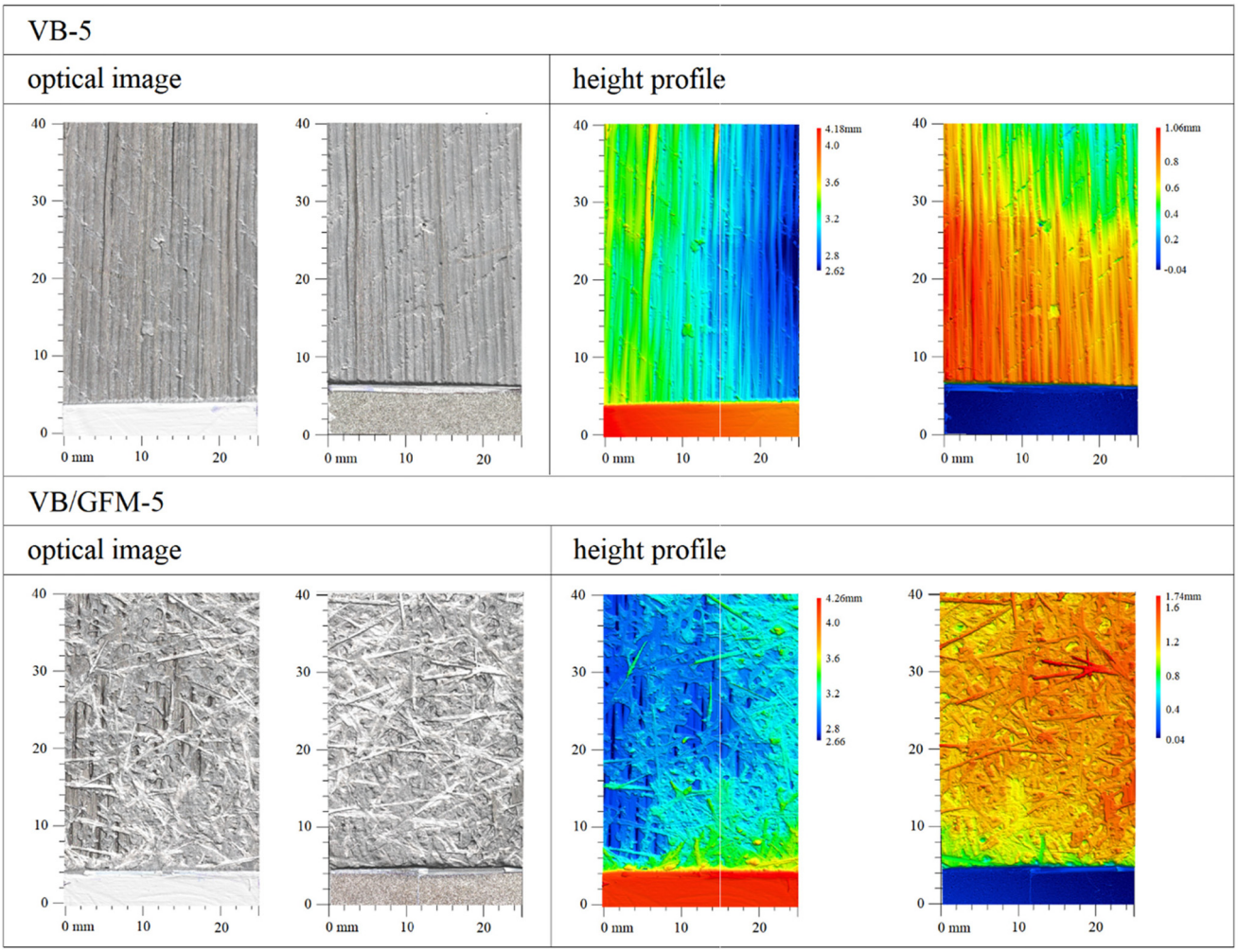


**Fig. 14.** Representative fracture surfaces of specimens manufactured using vacuum bagging under 40% mode II fracture.

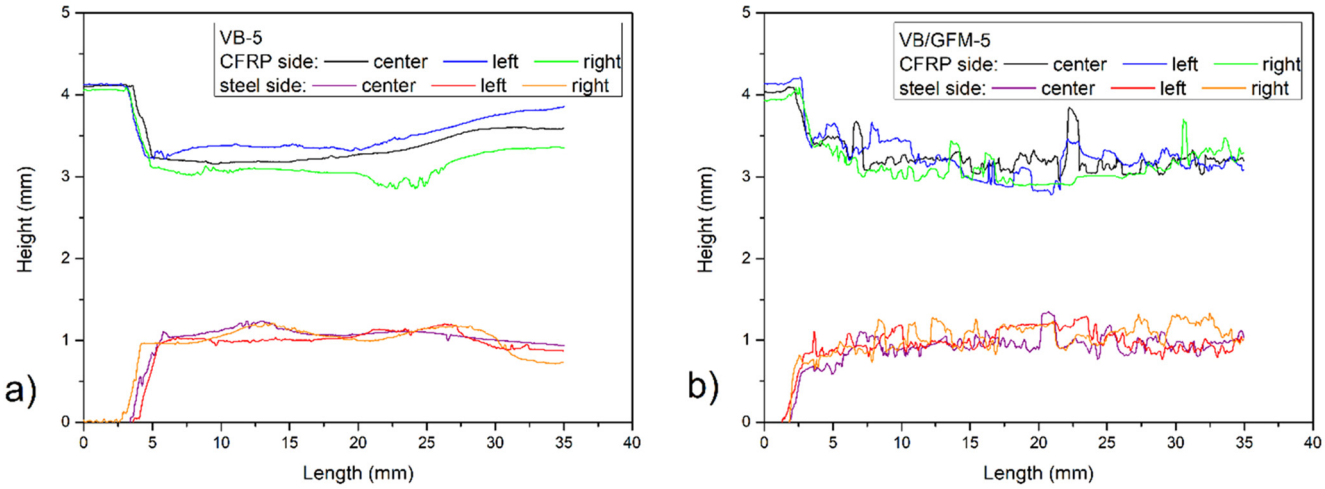


**Fig. 15.** Representative fracture height profiles of specimens manufactured using vacuum bagging under 40% mode II fracture (a) without and (b) with GFM.

These results are analogous to the previous cases (see Figs. 11 and 13). Therefore, the fracture partitioning ratio had no notable effect in the height profile of the fracture surfaces.

The roughness of the fracture surfaces was measured from an area of 10x10 mm at the center of the fracture surfaces. Table 4 presents the root mean square height (Sq) obtained from the CFRP and steel sides of the tested specimens. Results from every specimen revealed similar roughness in both sides of the crack. In general, cracks within the GFM showed rougher fracture surfaces. It is observed that specimen RP-2 presented a rougher surface compared with the others of the same design and manufacture process. This can be related to the more stepwise propagation (see Fig. 2) and higher fracture energy (see Fig. 6) obtained from this tested specimen.

**Table 4**
Roughness of the fracture surfaces.

| Specimen | $G_{II}/G$ | Adherend side | Root mean square height, Sq (μm) |
|---|---|---|---|
| RP-1 | 75% | CFRP | 88.4 |
| | | steel | 70.2 |
| RP-2 | 75% | CFRP | 135.9 |
| | | steel | 133.6 |
| RP-3 | 75% | CFRP | 71.8 |
| | | steel | 65.9 |
| RP-4 | 75% | CFRP | 84.5 |
| | | steel | 68.7 |
| RP/GFM-1 | 75% | CFRP | 150.0 |
| | | steel | 167.4 |
| RP/GFM-2 | 75% | CFRP | 129.4 |
| | | steel | 112.1 |
| RP/GFM-3 | 75% | CFRP | 121.4 |
| | | steel | 117.8 |
| RP/GFM-4 | 75% | CFRP | 144.9 |
| | | steel | 125.7 |
| VB-1 | 75% | CFRP | 59.5 |
| | | steel | 60.4 |
| VB-2 | 75% | CFRP | 68.8 |
| | | steel | 67.9 |
| VB-3 | 75% | CFRP | 97.6 |
| | | steel | 84.9 |
| VB/GFM-1 | 75% | CFRP | 149.8 |
| | | steel | 155.0 |
| VB/GFM-2 | 75% | CFRP | 184.5 |
| | | steel | 172.5 |
| VB/GFM-3 | 75% | CFRP | 136.8 |
| | | steel | 158.2 |
| VB-4 | 40% | CFRP | 91.3 |
| | | steel | 88.0 |
| VB-5 | 40% | CFRP | 88.6 |
| | | steel | 68.7 |
| VB/GFM-4 | 40% | CFRP | 169.5 |
| | | steel | 154.9 |
| VB/GFM-5 | 40% | CFRP | 163.9 |
| | | steel | 162.4 |

The relationship between the surface roughness and the fracture energy is presented in Fig. 16. The average surface roughness ($Sq_{ave}$), showed in the x-axis, is the average between the CFRP and steel fracture surfaces of the specimen. The data is clustered in three series: RP ($G_{II}/G$ = 75%), VB ($G_{II}/G$ = 75%) and VB ($G_{II}/G$ = 40%). For each of these three clustered series, it is observed a common trend of increasing the fracture energy with surface roughness as a result of inserting a layer of GFM. This can be observed by the positive slope of the three linear fits for all three clustered series. Specimens manufactured at room pressure and tested under 75% mode II fracture - RP ($G_{II}/G$ = 75%) show an increase of 49% in the $Sq_{ave}$ with the presence of GFM, which resulted in 89% increase in the $G_{ave}$. Specimens manufactured using vacuum bagging and tested under the same ratio - VB ($G_{II}/G$ = 75%) show an increase of 118% in the $Sq_{ave}$ with the presence of the GFM, which resulted in 170% increase in the $G_{ave}$. Therefore, specimens tested under the same fracture mode ratio, the ones manufactured using vacuum bagging produced higher fracture surface roughness and consequently higher fracture energy. Finally, in specimens manufactured with vacuum bagging and tested under a lower fracture mode ratio of 40% mode II - VB ($G_{II}/G$ = 40%), the $Sq_{ave}$ increased 93% with the insertion of the GFM but the $G_{ave}$ increased only 27%. Although the surface roughness increased in a similar extent for all specimens manufactured under vacuum bagging, the toughening effect is more evident under higher mode II fracture conditions.

### 4.3. Fractography

In order to better understand the effect of the manufacturing process on the fracture surface features, a fractography analysis was performed using a field emission scanning electron microscope (SEM) (JEOL JSM-7500F, Japan). Prior to examination, the samples were coated with a thin layer of gold (Au) using a sputter coater (Quorum Q300T D, United Kingdom). SEM images were obtained from the steel side of the fracture in magnification of 500x.

Fig. 17 shows representative SEM images of the fracture surface of the specimens without GFM. Specimens manufactured at room pressure and tested under 75% mode II presented a combination of cohe-

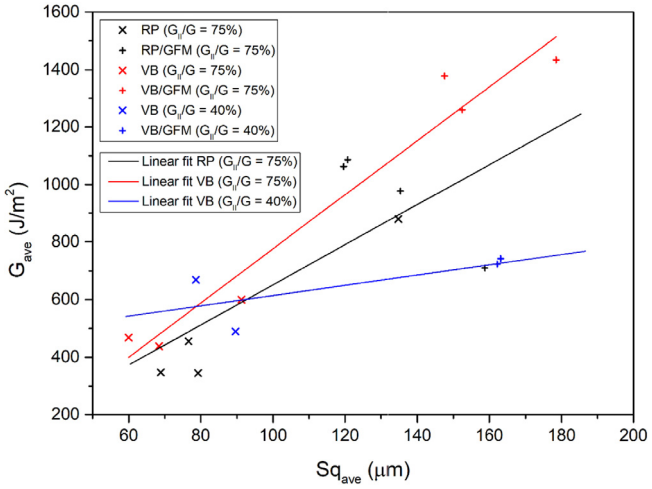


**Fig. 16.** Relationship between surface roughness and fracture energy.

sive and interlaminar failure within the first layer of carbon fibers, as shown in Fig. 17a. Similar failure modes are observed in Fig. 17b for specimens manufactured using vacuum bagging and tested under the same ratio. Nevertheless, the specimens tested under 40% mode II fracture presented dominant cohesive failure, as observed in Fig. 17c. These features explain the similar fracture energy of specimens without GFM from both manufacturing processes (RP and VB) and the slightly higher performance under 40% mode II fracture ratio (see Fig. 9). The increase in mode I fracture increases the cohesive failure mode within the adhesive layer. For mode II dominated fracture, cracks tend to propagate in the inner layer of the laminate. This relationship between fracture mode ratio and crack propagation path is also noticed in the literature [24].

Fig. 18 shows representative SEM images of the fracture surfaces of the specimens with an inserted layer of GFM. The glass fiber/matrix interactions are visible, showing the crack path inside the GFM. The fracture surfaces are significantly different from the ones without GFM, in Fig. 17, where the crack developed at the CFRP/adhesive interface. Fig. 18a shows the specimens manufactured at room pressure with GFM and tested with 75% mode II fracture. It is clearly displayed the presence of loose fibers and bare fibers. Specimens manufactured using vacuum bagging and tested under the same fracture mode ratio, shown in Fig. 18b, exhibited higher compaction and better fiber/matrix adhesion. This is a consequence of the vacuum pressure applied for consolidation of the composite during manufacture. A higher compaction of the mat contributes to an increased fracture performance [31], and, consequently, the toughening effect is more evident in specimens manufactured using vacuum bagging than at room pressure (see Fig. 9). Moreover, good fiber/matrix compaction is observed in Fig. 18c for a dominant mode I fracture, similar to the

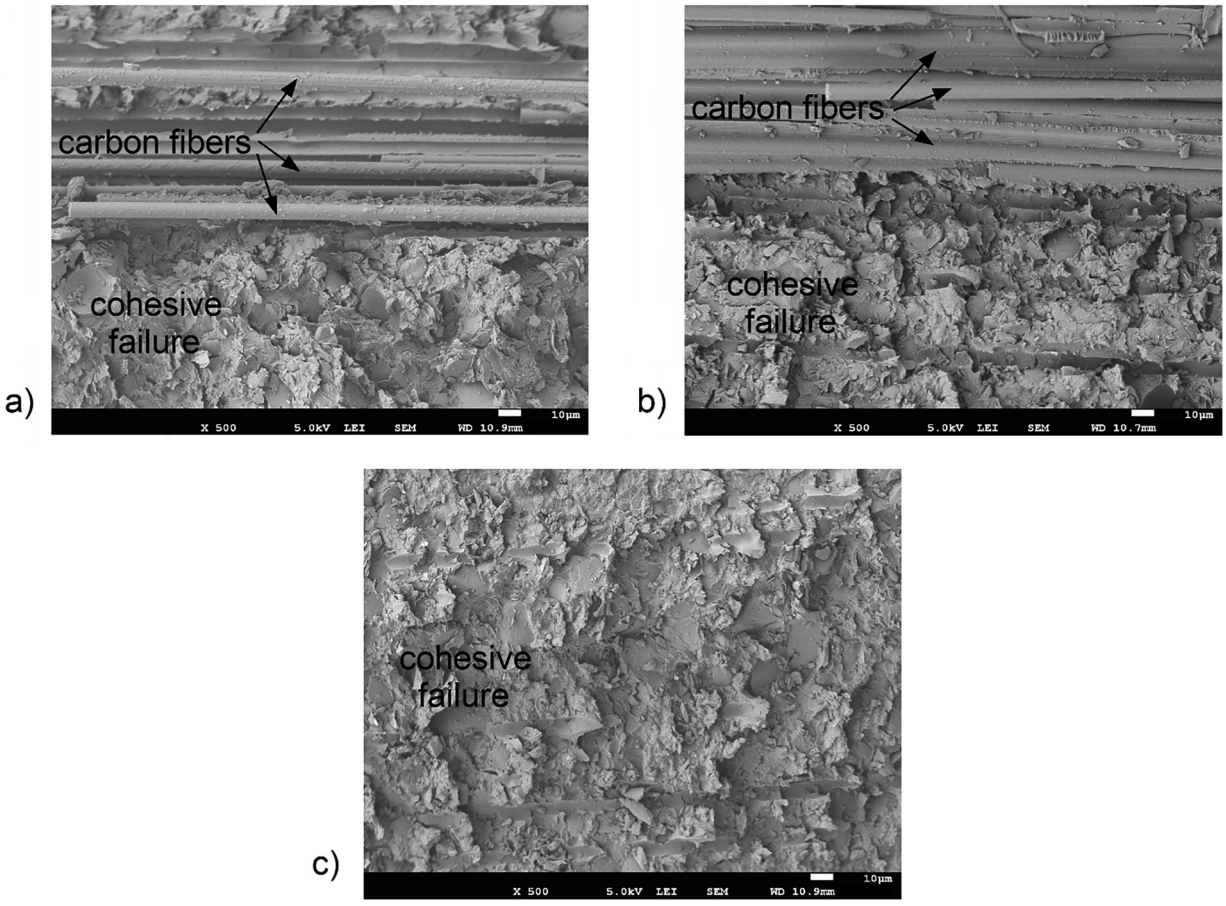


**Fig. 17.** SEM images of the steel side of specimens without GFM: (a) RP-4 ($G_{II}/G$ = 75%), (b) VB-2 ($G_{II}/G$ = 75%) and (c) VB-5 ($G_{II}/G$ = 40%).

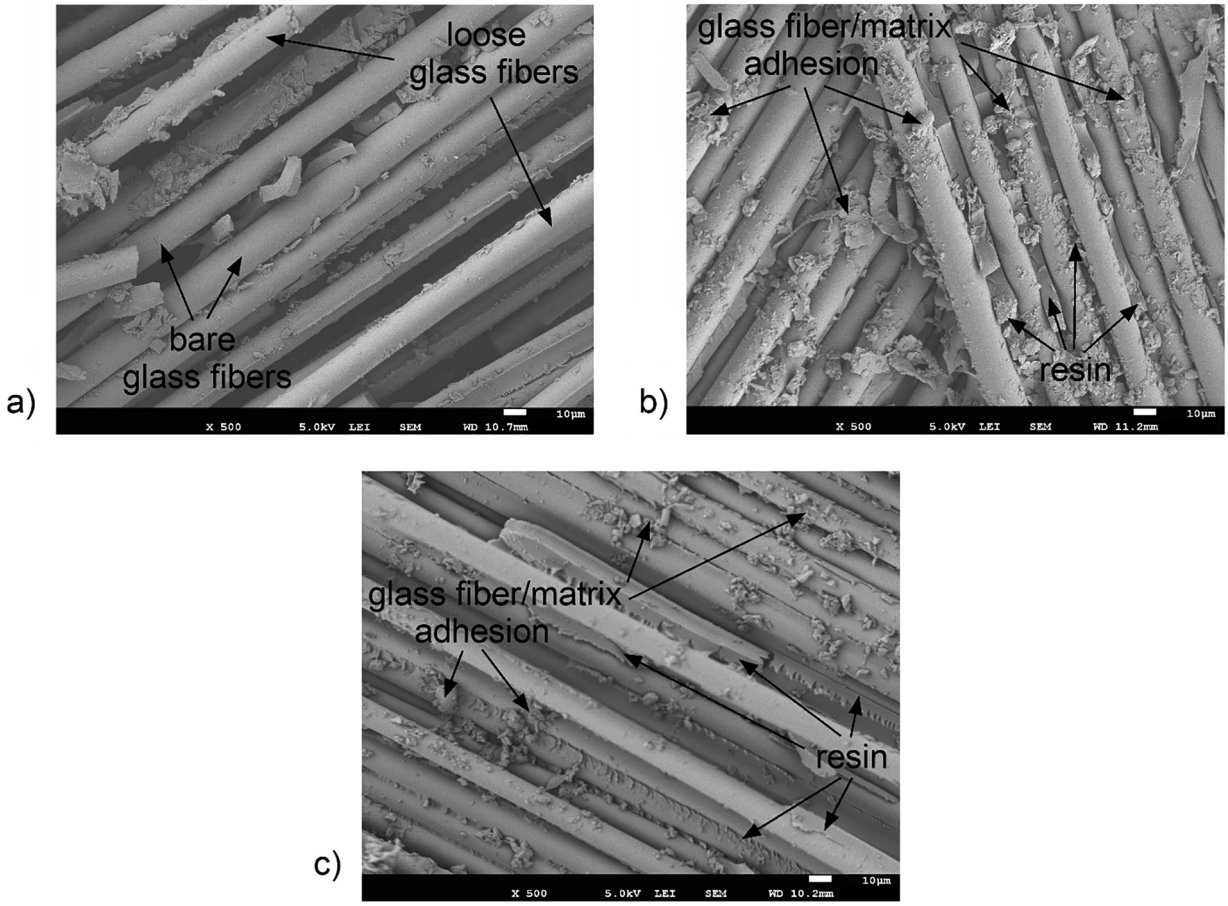


**Fig. 18.** SEM images of the steel side of specimens with GFM: (a) RP/GFM-2 ($G_{II}/G$ = 75%), (b) VB/GFM-3 ($G_{II}/G$ = 75%) and (c) VB/GFM-5 ($G_{II}/G$ = 40%).

case of high mode II fracture (Fig. 18b). Therefore, the inferior performance of specimens tested under 40% mode II regards only the loading conditions and not the failure mode.

## 5. Conclusion

The influence of a layer of glass fiber mat (GFM) inserted in a bi-material interface has been investigated as a toughening mechanism to improve the fracture performance of bonded structures. Composite-to-metal bonded specimens were manufactured by hand lay-up using two different consolidation processes: at room pressure or using vacuum bagging. The mixed-mode fracture behavior was evaluated under quasi-static loadings using the MMB test. Fracture toughening mechanisms were investigated through the test results and fractography analysis.

Crack tends to propagate in the interface between the adhesive layer and the upper arm of the specimen due to the higher stresses caused by the MMB loading configuration. In the case of a CFRP adherend without GFM, cohesive failure within the adhesive layer is the dominant failure mode under high mode I fracture while a combination of cohesive and interlaminar failure occurs in high mode II fracture conditions.

The insertion of a layer of GFM between adherends prevented the crack migration to the CFRP adherend and introduced a preferential crack propagation path within the GFM. The crack propagation within the GFM produced more irregular fracture surface profiles when compared to the specimens without GFM. A more irregular crack path resulted in higher fracture toughness due to the increase of the energy required for the crack to propagate. Therefore, the adjacent composite layer to the adhesive interface has an important role in the fracture performance of the bonded joint since it affects the crack propagation path.

The manufacturing process affected the performance of the specimens with GFM. The vacuum bagging technique produced a better fiber/matrix compaction of the GFM and resulted in rougher fracture surfaces when compared to room pressure. On the other hand, no change was observed in the fracture surfaces of specimens without GFM despite the manufacturing process. The relationship between fracture surface roughness and fracture performance is observed in both manufacturing processes although the toughening effect is more evident in higher mode II fracture conditions.

The insertion of a layer of GFM is expected to increase the fracture performance of composite repairs in metal structures. The use of vacuum pressure in the consolidation of the composite, when feasible, is recommended for optimizing the fracture performance of the bonded structure.

Even though the values measured for the fracture toughness appear coherent, only the principles of LEFM have been considered for the evaluation of the fracture performance. The non-linearity effects of the plastic zone developed around the crack tip has not been taken into account and may be contemplated in future studies. The integration of a non-linear analysis may potentially improve the understanding over the fracture behavior of composite-to-metal bonded joints.

## CRediT authorship contribution statement

**Marcio Moreira Arouche:** Conceptualization, Methodology, Formal analysis, Investigation, Writing - original draft, Visualization, Pro-

ject administration. **Sofia Teixeira de Freitas:** Conceptualization, Methodology, Supervision, Funding acquisition. **Silvio de Barros:** Conceptualization, Methodology, Supervision, Funding acquisition.

## Declaration of Competing Interest

The authors declare that they have no known competing financial interests or personal relationships that could have appeared to influence the work reported in this paper.

## Acknowledgements

This work was supported by the Coordenação de Aperfeiçoamento de Pessoal de Nível Superior - Brasil (CAPES), Conselho Nacional de Desenvolvimento Científico e Tecnológico (CNPq), Fundação Carlos Chagas Filho de Amparo à Pesquisa do Estado do Rio de Janeiro (FAPERJ) [001], and the Netherlands Organisation for Scientific Research [project number 14366].

## Data Availability

The raw/processed data required to reproduce these findings cannot be shared at this time as the data also forms part of an ongoing study.

## References

[1] Budhe S, Banea MD, de Barros S, da Silva LFM. An updated review of adhesively bonded joints in composite materials. Int J Adhes Adhes 2017;72:30–42.
[2] Mangalgiri PD. Composite materials for aerospace applications. Bull Mater Sci 1999;22(3):657–64.
[3] Budhe S, Banea MD, de Barros S. Bonded repair of composite structures in aerospace application: a review on environmental issues. Appl Adhes Sci 2018;6:3.
[4] Taub AI, Krajewski PE, Luo AA, Owens JN. The evolution of technology for materials processing over the last 50 years: The automotive example. JOM 2007;59(2):48–57.
[5] Van Den Einde L, Zhao L, Seible F. Use of FRP composites in civil structural applications. Constr Build Mater 2003;17:389–403.
[6] Katnam KB, da Silva LFM, Young TM. Bonded repair of composite aircraft structures: A review of scientific challenges and opportunities. Prog Aerosp Sci 2013;61:26–42.
[7] Arouche MM, Budhe S, Alves LA, Teixeira de Freitas S, Banea MD, de Barros S. Effect of moisture on the adhesion of CFRP-to-steel bonded joints using peel tests. J Braz Soc Mech Sci Eng 2018;40(10).
[8] Arouche MM, Budhe S, Banea MD, Teixeira de Freitas S, de Barros S. Interlaminar adhesion assessment of carbon-epoxy laminates under salt water ageing using peel tests. Proc IMechE Part L 2019;233(8):1555–63.
[9] Rudawska A. Comparison of the adhesive joints' strength of the similar and dissimilar systems of metal alloy/polymer composite. Appl Adhes Sci 2019;7(1). https://doi.org/10.1186/s40563-019-0123-x.
[10] De Barros S, Banea MD, Budhe S, De Siqueira CER, Lobão BSP, Souza LFG. Experimental analysis of metal-composite repair of floating offshore units (FPSO). J Adhes 2017;93(1-2):147–58.
[11] da Costa Mattos HS, Reis JML, Paim LM, da Silva ML, Lopes Junior R, Perrut VA. Failure analysis of corroded pipelines reinforced with composite repair systems. Eng Fail Anal 2016;59:223–36.
[12] McGeorge D, Echtermeyer AT, Leong KH, Melve B, Robinson M, Fischer KP. Repair of floating offshore units using bonded fibre composite materials. Compos A Appl Sci Manuf 2009;40(9):1364–80.
[13] Meniconi LC, Lana LD, Morikawa SR. Experimental fatigue and aging evaluation of the composite patch repair of a metallic ship hull. Appl Adhes Sci 2014;2:27.
[14] DNV-RP-C301 – Design, Fabrication, Operation and Qualification of Bonded Repair of Steel Structures, Det Norske Veritas AS, 2015.
[15] Chaves FJP, da Silva LFM, de Moura MFSF, Dillard DA, Esteves VHC. Fracture mechanics tests in adhesively bonded joints: A literature review. J Adhes 2014;90(12):955–92.
[16] Reeder JR, Crews Jr JH. Mixed-mode bending method for delamination testing. AIAA J 1990;28(7):1270–6.
[17] Reeder JR, Crews Jr JH. Redesign of the mixed-mode bending delamination test to reduce non-linear effects. J Compos Technol Res 1992;14(1):12–9.
[18] Pereira AB, de Morais AB. Mixed mode I+II interlaminar fracture of carbon/epoxy laminates. Compos A Appl Sci Manuf 2008;39(2):322–33.
[19] Shahverdi M, Vassilopoulos AP, Keller T. Mixed-mode I/II fracture behavior of asymmetric adhesively-bonded pultruded composite joints. Eng Fract Mech 2014;115:43–59.
[20] Liu Z, Gibson RF, Newaz GM. The use of a modified mixed mode bending test for characterization of mixed-mode fracture behavior of adhesively bonded metal joints. J Adhes 2002;78(3):223–44.
[21] Stamoulis G, Carrere N, Cognard JY, Davies P, Badulescu C. On the experimental mixed-mode failure of adhesively bonded metallic joints. Int J Adhes Adhes 2014;51:148–58.
[22] Quispitupa A, Berggreen C, Carlsson LA. On the analysis of a mixed mode bending sandwich specimen for debond fracture characterization. Eng Fract Mech 2009;76(4):594–613.
[23] Arouche MM, Wang W, Teixeira de Freitas S, de Barros S. Strain-based methodology for mixed-mode I+II fracture: A new partitioning method for bi-material adhesively bonded joints. J Adhes 2019;95(5-7):385–404.
[24] Quispitupa A, Berggreen C, Carlsson LA. Face/core interface fracture characterization of mixed mode bending sandwich specimens. Fatigue Fract Eng Mater Struct 2011;34:839–53.
[25] Kim BW, Mayer AH. Influence of fiber direction and mixed-mode ratio on delamination fracture toughness of carbon/epoxy laminates. Compos Sci Technol. 2003;63(5):695–713.
[26] Andersons J, König M. Dependence of fracture toughness of composite laminates on interface ply orientations and delamination growth direction. Compos Sci Technol 2004;64(13-14):2139–52.
[27] Sela N, Ishai O. Interlaminar fracture toughness and toughening of laminated composite materials: a review. Composites 1989;20(5):423–35.
[28] Kuwata M, Hogg PJ. Interlaminar toughness of interleaved CFRP using non-woven veils: Part 1. Mode-I testing. Compos A Appl Sci Manuf 2011;42(10):1551–9.
[29] Hosseini MR, Taheri-Behrooz F, Salamat-talab M. Mode I interlaminar fracture toughness of woven glass/epoxy composites with mat layers at delamination interface. Polym Test 2019;78:105943.
[30] Kuwata M, Hogg PJ. Interlaminar toughness of interleaved CFRP using non-woven veils: Part 2. Mode-II testing. Compos A Appl Sci Manuf 2011;42(10):1560–70.
[31] Boccaccini AR, Winkler V. Fracture surface roughness and toughness of Al2O3-platelet reinforced glass matrix composites. Compos A Appl Sci Manuf 2002;33(1):125–31.
[32] Lundsgaard-Larsen C, Berggreen C, Carlsson LA. Tailoring sandwich face/core interfaces for improved damage tolerance – Part II: Experiments. Appl Compos Mater 2010;17:621–37.
[33] Karger-Kocsis J, Harmia T, Czigány T. Comparison of the fracture and failure behavior of polypropylene composites reinforced by long glass fibers and by glass mats. Compos Sci Technol 1995;54(3):287–98.
[34] Huang B-Z, Hu X-Z, Liu J. Modelling of inter-laminar toughening from chopped Kevlar fibers. Compos Sci Technol 2004;64(13-14):2165–75.
[35] Kopp J-B, Schmittbuhl J, Noel O, Lin J, Fond C. Fluctuations of the dynamic fracture energy values related to the amount of created fracture surface. Eng Fract Mech 2014;126:178–89.
[36] Sun Z, Shi S, Hu X, Guo Xu, Chen J, Chen H. Short-aramid-fiber toughening of epoxy adhesive joint between carbon fiber composites and metal substrates with different surface morphology. Compos B Eng 2015;77:38–45.
[37] Teixeira de Freitas S, Banea MD, Budhe S, de Barros S. Interface adhesion assessment of composite-to-metal bonded joints under salt spray conditions using peel tests. Compos Struct 2017;164:68–75.